Progress In Electromagnetics Research B, Vol. 93, 169–194, 2021

Optimization Design Methodology of Broadband or Multiband Antenna for RF Energy Harvesting Applications

Reham M. Yaseen, Dhirgham K. Naji*, and Amina M. Shakir

Abstract—In this paper, a patch antenna (PA) and its self-complementary structure, slot antenna (SA) are proposed and designed for directly matching the impedance of a rectifier at 2.45 GHz resonance frequency. The structures of these antennas comprise three sections, meandered-line, spiral, and a double-folded geometries, which make their geometrical parameters to be varied in easy manner according to design equations. In order to enhance both the desired level of a complex reflection coefficient of antenna at given resonance frequencies and the specified lower and higher frequencies constituting the impedance frequency bands, a new fitness function is presented. This fitness function is applied in designing broadband or multiband antennas having approximately perfect conjugate impedance matching with the impedance of a rectifier suitably used for RF Energy Harvesting (RFEH) application. An optimization design methodology based on two programs operating in synchronous manner, the particle swarm optimization (PSO) implemented in MATLAB simulation tool and a CST MWS Electromagnetic (EM) solver, is applied to the designed PA as an illustrative example. The simulation results reveal that our design methodology is helpful to obtain an optimized PA (OPA) having good impedance matching at the desired resonance frequency along with appropriate band. Measured result of the fabricated prototype is in good agreement with the simulated ones. Moreover, acceptable features such as small size, omnidirectional radiation, and broadband operation satisfy the (2.4–2.5 GHz) WLAN band, which strongly makes the OPA a good candidate for RFEH applications.

1. INTRODUCTION

Radio frequency (RF) energy harvesting (EH) has gained considerable attention as a way to allow self-powered wireless communication networks. A conventional rectenna (rectifier + antenna) is a typical RFEH system which consists of an antenna, a rectifier, and an impedance matching network [1–3]. Recently, there has been great interest in eliminating the use of matching networks because of their challenging design for broadband and multiband applications. Moreover, the matching network adding more complexity, larger size, and more losses that affect the performance of the overall rectenna system [2–9]. However, high power conversion efficiency (PCE) is obtained for rectennas having antennas to directly match their impedances with the rectifier's impedance compared to rectennas with stand-alone matching networks [10, 11].

In general, conventional RFEH systems with impedance matching networks, as shown in Fig. 1(a), normally consist of five different parts: a receiving antenna, a band pass filter, an impedance matching network, a rectifier, and a resistive load. On the other hand, an RFEH system without using impedance matching network, as shown in Fig. 1(b), comprises only three parts, a receiving antenna, a rectifier, and a resistive load [6]. As shown in Fig. 1(a), in the conventional rectenna configuration, the input impedance of the antenna matched with 50 Ω impedance of the rectifier leads to either narrow operating

Received 1 July 2021, Accepted 13 September 2021, Scheduled 28 September 2021
* Corresponding author: Dhirgham Kamal Naji (dhrgham.kamal@gmail.com).
The authors are with the Department of Electronic and Communications Engineering, College of Engineering, Al-Nahrain University, Baghdad, Iraq.

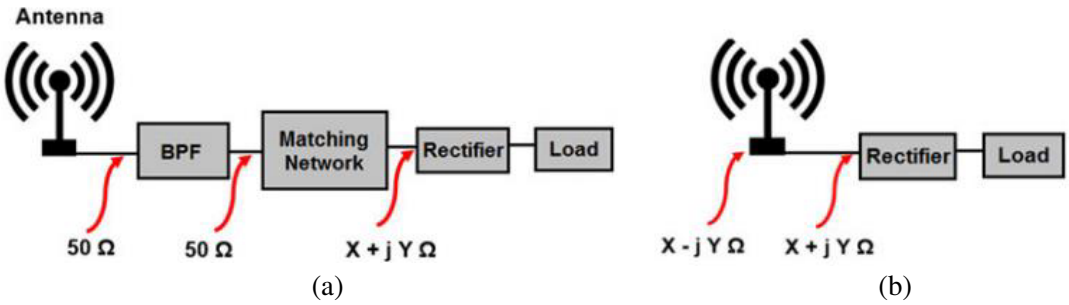

Figure 1. Configuration of (a) a conventional rectifying antenna system with impedance matching networks and (b) rectifying antenna without using impedance matching networks [6].

bandwidth [12] or low PCE over the broadband [13]. Therefore, as shown in Fig. 1(b), for delivering the received RF power at different frequency bands with a high PCE to the rectifier, the impedance matching network should be removed or simplified.

Among antenna types, microstrip PA and SA are attractive designs offering several features for RFEH systems [14–21], including low profile, relatively easy design, the reduction in fabrication cost, and the miniaturization in physical dimensions of antennas in comparison with the wavelengths of the desired frequencies. Additional important features for antennas suitably used in RFEH applications are complex reflection coefficient and impedance frequency bands [22]. In recent reports, different PAs with matching network elimination have been proposed for rectennas, such as hollowed-out square loop antenna [8], crossed off-center-fed dipole antenna [6], and a pair of pentagonal loops [23]. Therefore, rectennas having compact sizes and improved PCE performance over the broadband or various frequency bands are successively reported in previous literatures. However, most of these designs are either large in size, due to using matching networks or having complex structures. Thus, it is desirable to use an antenna having two features, miniaturized size with simpler structure and input impedance easily matched with the impedance of the rectifier. To satisfy the above-mentioned features, miniaturization and impedance matching, antenna optimization is applied in this work for designing a meander line antenna loaded with spiral and folded shaped structure. Therefore, instead of merely meanders, spiral and folded-shaped end loads are also utilized, reducing the overall size of an antenna without influencing in its performance.

Antenna optimization is a process that aims at creating an antenna having small physical size with good features in terms of quality performance, cost effectiveness, and ease of service. This includes the appropriate selection of an objective (fitness) function, constraints, and antenna's design variables that enter the optimization process. Thus, in order to successfully obtain the optimal solution of an antenna optimization problem, a set of goals must be satisfied simultaneously. Therefore, an engineering problem such as antenna optimization can be considered as an efficient procedure for making the designed antennas optimized for satisfying the required characteristics mentioned above [24]. Several widely-known meta-heuristic algorithms have been adopted in antenna optimization such as Genetic Algorithm (GA) [25–27], Particle Swarm Optimization (PSO) [28–33], simulated annealing [34], and invasive weed optimization (IWO) [35–37]. The antennas presented in these references demonstrate that the PSO algorithm has several features, such as easy implementation and suitability for use in the design of those antennas including single- and multi-objective optimization problems among other algorithms. Thus, the PSO is adopted in this work for solving the optimization problem.

This paper presents a new innovative optimization methodology for designing antennas which takes into account both the level of resonance(s) frequency (frequencies) and the lower and upper frequency (frequencies) for the -3 dB-Γ impedance bandwidth. To our knowledge, there is no work in the open literature that takes into account these points in the design. Our design method is simple to implement, and it is comprehensively discussed as both the mathematical equations and design implementation which make it easily to understand by the others.

The design of antennas without matching networks suitably for use in rectenna systems is still a challenging task for researchers. Therefore, the aim of this work is to design antennas without matching

network suitably for use in RFEH applications via optimization methodology. This aim is done in two steps. Firstly, PA and its self-complementary structure, SA, are proposed and designed to operate effectively at 2.45 GHz. The input impedance of PA and SA are easily tuned and directly conjugate-matched to the desired input impedance of a rectifier ($6-j170\,\Omega$). A low-cost FR4 substrate with height of 0.8 mm is used in simulation and fabrication of antennas having compact sizes of $28 \times 10.25\,\text{mm}^2$ and $27.36 \times 10.25\,\text{mm}^2$ for PA and SA, respectively. A CST Microwave Studio (CST MWS) is used to model and analyze the designed antennas. Simulation results in terms of real and imaginary parts of antenna impedance along with the complex reflection coefficient (Γ) are compared with the measured counterparts, and a close agreement between them has been obtained. Secondly, we present a new fitness function that takes into account both the desired level of Γ at given resonance frequencies and the specified lower and higher frequencies for the -3 dB-Γ impedance bandwidth. This fitness function is applied in designing a broadband or multiband antennas having approximately perfect conjugate impedance matching to the impedance of a rectifier. The PSO implemented in MATLAB in conjunction with CST simulator is applied to the PA designed previously as an initial PA (IPA) design from which the optimized PA (OPA) is achieved. At the end of optimization, more than -15 dB of Γ is obtained compared with $\Gamma = -5.74$ dB for IPA at 2.45 GHz. Moreover, OPA has more than 50% of -3 dB-Γ impedance bandwidth ranging from 2.4 to 2.5 GHz in comparison with IPA counterpart which operates in 2.43–2.47 GHz band. The OPA is fabricated on an FR4 substrate with an overall size of $32.8 \times 9.7 \times 0.8\,\text{mm}^3$, and the measured results in terms of -3 dB-Γ impedance bandwidth agree well with the simulated ones.

The rest of this paper is structured as follows. Section 2 presents the design, analysis and performance of the proposed antennas. Section 3 discusses the simulated and measured results. Section 4 describes in detail the optimization design methodology applied to achieve a feasible solution of the optimized antenna. Section 5 outlines the simulated and measured results of the fabricated proposed optimized antenna and a comparison of its features against the related previous works. Finally, Section 6 offers a conclusion for our findings of this work.

2. DESIGN, ANALYSIS AND PERFORMANCE OF THE PROPOSED ANTENNAS

2.1. Geometry of the Proposed Antennas

Figures 2(a) and (b) show the geometries of the proposed antennas, PA, and its complementary counterpart SA, respectively. Three sections, meander-line, spiral and double-folded geometries are connected together to constitute the radiating element of PA and SA, either as conductor patch strips or their complementary slot-loaded strips, respectively.

As seen in Fig. 2, fifteen geometry parameters denoted as $w_1, ..., w_{10}$ and $l_1, ..., l_5$ are considered as design parameters. Thus, 15 design parameters are allowed to be varied within specified ranges by a method of trial-and-error procedure for conjugate-matched antenna impedance Z_A with the impedance of load Z_L. These two antennas are printed on an FR4 substrate with overall dimensions $W_{sub} \times L_{sub}$ and (thickness $h_{sub} = 0.8$ mm, relative permittivity $\epsilon_r = 4.3$, and tangent loss 0.025). An Electromagnetic (EM) solver, CST Microwave Studio is used for parametric analyses and performance evaluation of antennas.

2.2. Evolution Design and the Working Principle of the Antennas

This section presents the design concept of the proposed PA and SA depicted in Fig. 2 by a trail-and-error procedure for satisfying their impedances to be conjugate matched with the load impedance. As stated before, 15 design variables are considered as dependent geometric parameters which were used for dealing with the horizontal and vertical spacing between the strips or slots, $w_1, ..., w_{10}$ and $l_1, ..., l_5$, respectively. A geometric parameter, namely the width of a strip or slot (t) represents the main or an independent design parameter that influences the antennas' performances and their overall substrate dimensions $W_{sub} \times L_{sub} \times h_{sub}$. As shown in Fig. 2, the impedance of the proposed antennas can be easily controlled by using an appropriate value for each one of the three dimensional parameters (w_0, a, b) specifying the region at which the rectifier circuit is placed. The relation among dependent

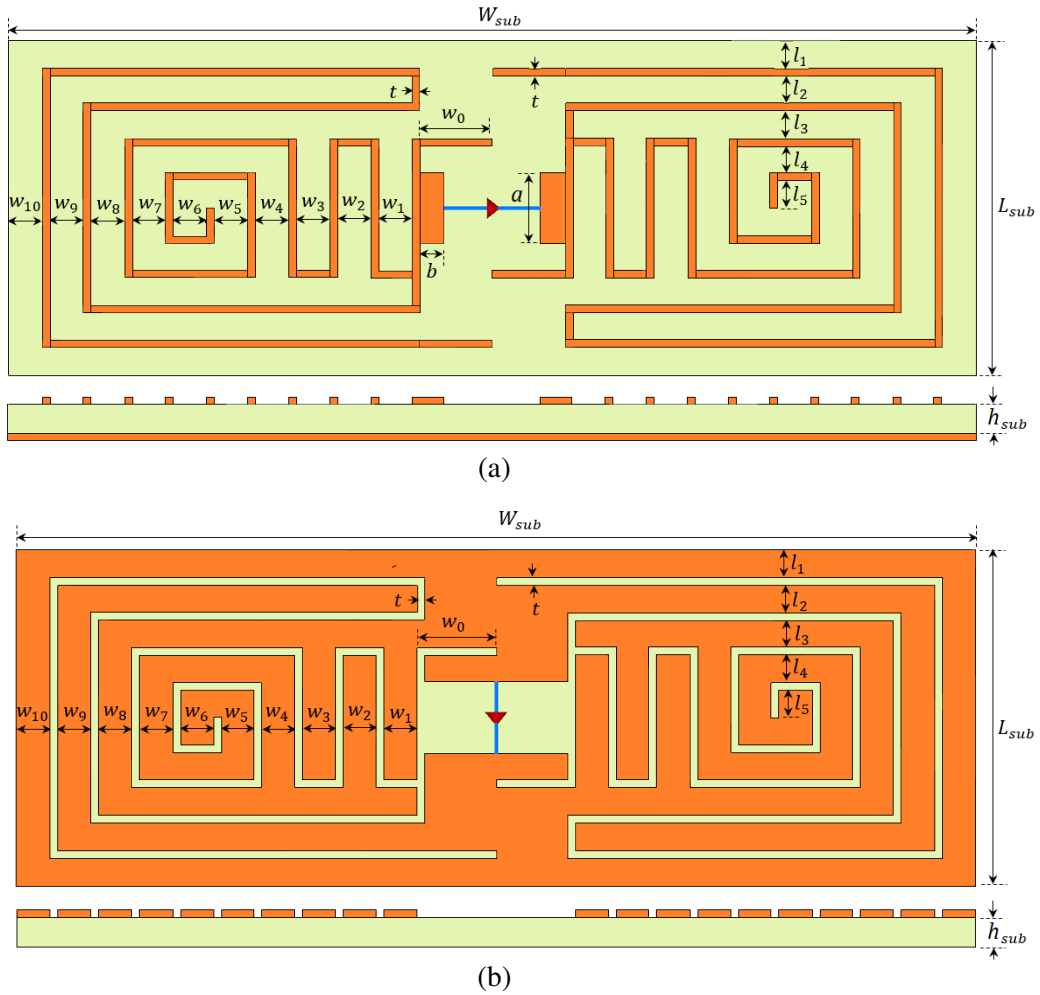

Figure 2. Layout of the proposed antennas. (a) Patch antenna (PA). (b) Slot antenna (SA).

and independent variables is written as:

$$W_{sub} = 2\left(10t + \sum_{i=0}^{10} w_i\right) \tag{1a}$$

$$L_{sub} = 2\left(4t + \sum_{j=1}^{5} l_j\right) \tag{1b}$$

where w_i and l_j are related to t by the relations:

$$w_i = nt, \quad 1 \le n \le 6, \quad i = 1, 2, ..., 10 \tag{2a}$$

$$l_j = mt, \quad 1 \le m \le 8, \quad j = 1, 2, ..., 5 \tag{2b}$$

Table 1 lists the summary of geometric parameters of the proposed antennas in three categories; fixed, dependent, and independent (as design parameters) besides their boundaries. As seen in this table, the minimum and maximum dimensions of the proposed antennas ($W_{sub} \times L_{sub}$) are (18 mm × 9 mm) and (48 mm × 26.4 mm), respectively when the dependent parameters are swept within their allowed limits.

A trial-and-error design approach via CST MWS is applied to design the proposed antennas, as each one of the 15 geometric parameters is allowed to be swept within the allowed range, as displayed in Table 1. The main objective of antenna design is to directly conjugate match its input impedance Z_A with the complex impedance Z_L of a specific rectifier (HSMS-286C). A 2.45 GHz resonance frequency, f_r, is set to allow an antenna to be successfully designed to have a real resistance R_A to match the

Table 1. Summary dimensions of the proposed antenna geometric parameters. (All length dimensions in mm) and (n and m are constants).

Fixed Parameters	$w_0 = 3.0\,\text{mm}$, $a = 3.0\,\text{mm}$, $b = 1.0\,\text{mm}$, $h_{sub} = 0.8\,\text{mm}$
Dependent Parameter	$t = 0.3\,\text{mm}$
Independent Parameters	$w_i = nt$, $i = 1, 2, ..., 10$ (10 variables) $l_j = mt$, $j = 1, 2, ..., 5$ (5 variables)
	W_{sub}, L_{sub} (2 variables)
Boundaries	$n \in [1, 6] \Rightarrow w_i \in [0.3, 1.8]$ for $i = 1, 2, ..., 10$ $m \in [1, 8] \Rightarrow l_j \in [0.3, 2.4]$ for $j = 1, 2, 3$ $m \in [4, 8] \Rightarrow l_j \in [1.2, 2.4]$ for $j = 4, 5$ $W_{sub} \in [18, 48]$, $L_{sub} \in [9.0, 26.4]$

Table 2. Final dimensions of the proposed antennas PA and SA.

Parameter	Value (mm)		Parameter	Value (mm)	
	PA	SA		PA	SA
W_{sub}	28.82	27.36	w_9	1.08	1.08
L_{sub}	10.50	10.52	w_{10}	1.08	1.08
h_{sub}	0.80	0.80	l_1	0.81	0.81
w_1	0.43	0.43	l_2	0.81	0.81
w_2	0.43	0.43	l_3	0.81	0.81
w_3	1.08	0.43	l_4	0.81	0.81
w_4	0.43	1.08	l_5	0.81	0.81
w_5	0.64	0.57	w_o	3.00	3.00
w_6	1.08	1.08	a	3.00	3.00
w_7	1.08	1.08	b	1.00	-
w_8	1.08	1.08	t	0.30	0.30

rectifier resistance $R_L = 6\,\Omega$, and an imaginary impedance X_A is conjugate matched to $X_L = -j170\,\Omega$ at $f_r = 2.45\,\text{GHz}$. Therefore, the goal of designing the antenna is that its magnitude of complex reflection coefficient $|\Gamma|$ in dB

$$|\Gamma| = 20 \log \left[\frac{(R_A - R_L)^2 + (X_A + X_L)^2}{(R_A + R_L)^2 + (X_A + X_L)^2} \right] \text{ (dB)} \tag{3}$$

is to be minimum at f_r when $R_A = R_L$ and $X_A = -X_L$.

Table 2 illustrates the final geometrical parameters of the designed antennas (PA and SA), and Fig. 3 depicts their performances in terms of $|\Gamma|$ and input impedance. As shown in Table 2 and

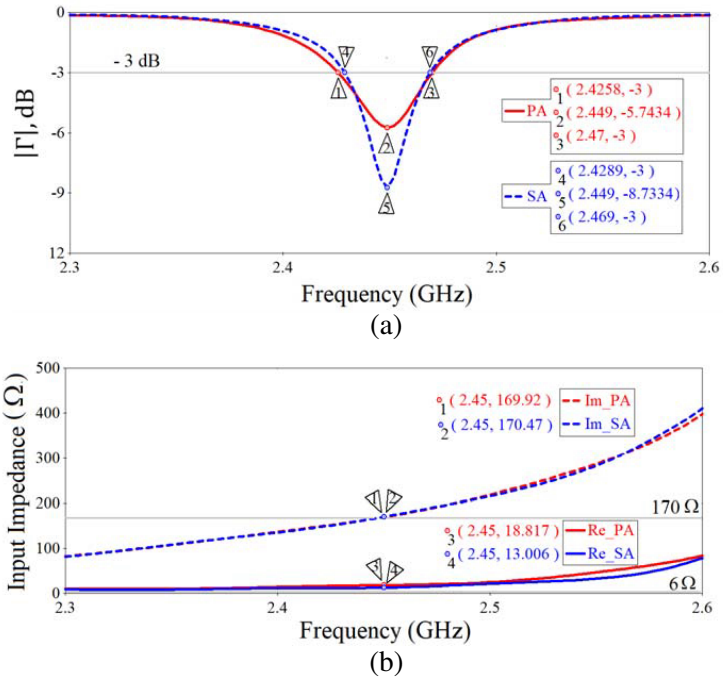

Figure 3. The performance proposed antennas, PA and SA. (a) The complex reflection coefficient. (b) Input impedance, Im (imaginary), Re (real).

Table 3. Simulated performance of the proposed antennas, PA and SA.

Antenna type	f_r (GHz)	$\|\Gamma\|\|_{f_r}$ (dB)	f_l (GHz)	f_h (GHz)	$R_A\|_{f_r}$ (Ω)	$X_A\|_{f_r}$ (Ω)
PA	2.445	−5.74	2.426	2.470	18.81	169.92
SA	2.449	−8.73	2.429	2.469	13.00	170.74

Fig. 3, the two antennas have almost the same geometrical parameters, performance, and impedance matching characteristic. Table 3 summarizes the main results of PA and SA in terms of resonance frequency (f_r), complex reflection coefficient $|\Gamma|$ at f_r, −3 dB bandwidth, lower frequency (f_l), and higher frequency (f_h), besides antenna resistance and reactance (R_A) and (X_A) at f_r, respectively. As noticed in Table 3, PA and its complementary counterpart SA have nearly identical performance in terms of resonance frequency, −3 dB bandwidth, and input impedance, Reactances are approximately equal to the conjugate of rectifier reactance (−170 Ω), but resistances are in good agreement and nearly equal to rectifier resistance (6 Ω).

2.3. Evolution Design Steps of Proposed Patch Antenna

In this section, the evolution design steps of the proposed PA are presented. The design steps of SA are similar to that of PA. Two antennas, namely, meander dipole PA (MDPA), meander and spiral PA (MSPA), besides the proposed PA are shown in Fig. 4. These three antennas have the same overall dimensions (28.82 mm × 10.50 mm) and are printed on the front side of FR substrate of height 0.8 mm. The MDA, as shown in Fig. 4(a), has only a meander line structure equally horizontally-spaced between its turns, i.e., $w_i = 0.43$ mm, $i = 1, 2, ..., 13$. This antenna resonates at $f_r = 3.42$ GHz with complex reflection coefficient $|\Gamma||_{f_r} = -5.16$ dB as seen in Fig. 5. This frequency is larger than the desired frequency of 2.45 GHz, thus the spiral's strips are added to the meander line to produce MSDA as shown in Fig. 4(b). This antenna resonates at 3.16 GHz with $|\Gamma|$ of −5.45 dB (see Fig. 5), and the

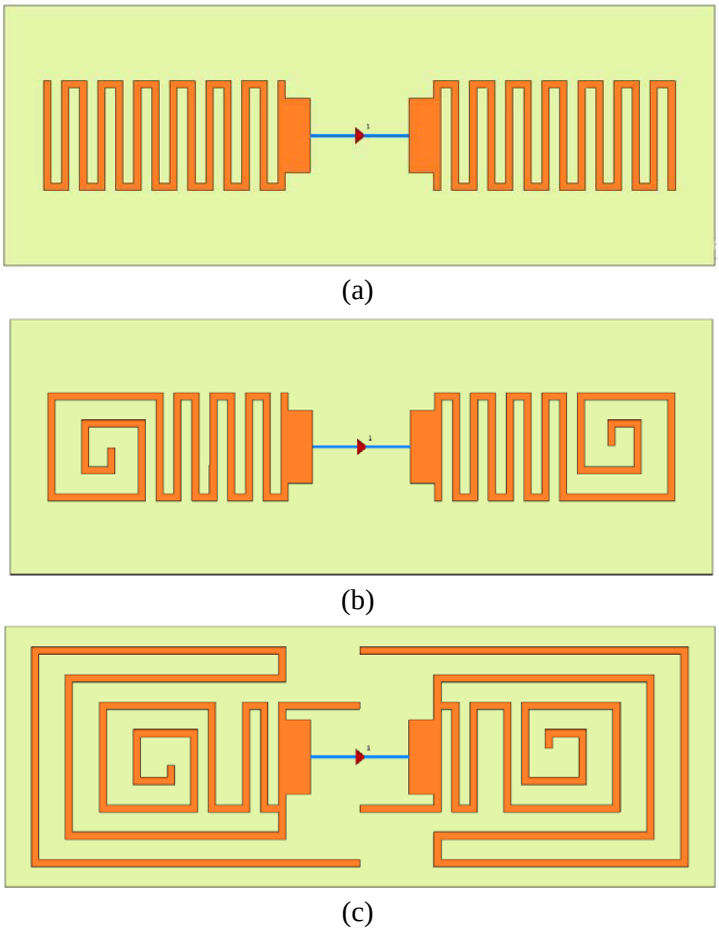

Figure 4. Evolution steps of proposed PA, (a) MPA, (b) MSPA, (c) the proposed PA.

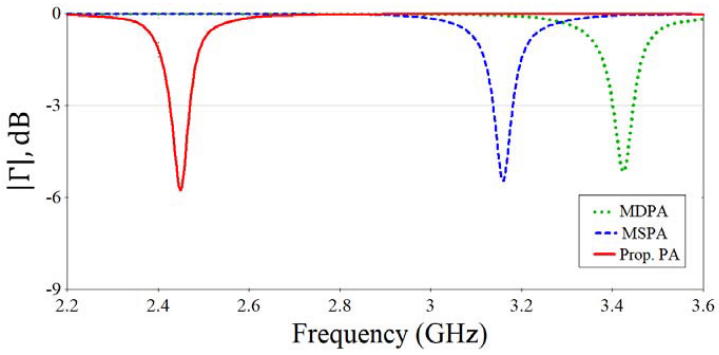

Figure 5. Simulated reflection coefficient $|\Gamma|$ versus frequency characteristics.

proposed PA is designed to achieve the desired $f_r = 2.45\,\text{GHz}$.

As noticed in Fig. 5, the proposed PA is successfully operated at 2.45 GHz by adding a double folded-dipole structure to the meander and spiral geometries. Therefore, instead of using only a meander line, spiral ending strips loaded by a double-folded structure are used herein as a technique to significantly reduce the resonance frequency of PA without enlarging its occupied size.

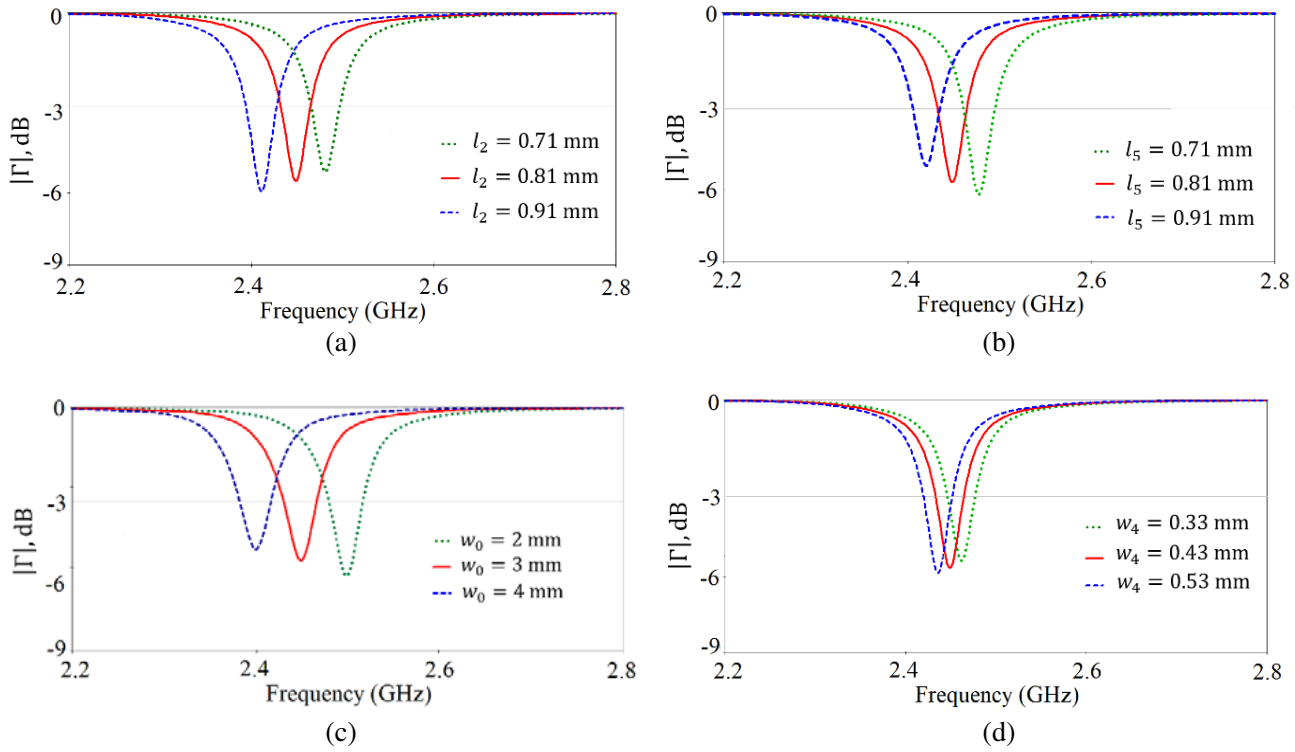

Figure 6. Simulated $|\Gamma|$ by varying some geometric parameters. (a) l_2, (b) l_5, (c) w_0, (d) w_4.

2.4. Parametric Analysis

In order to investigate the operation principle of PA, the impact of varying some spiral, meander line, and folded-shaped parameters on antenna reflection coefficient $|\Gamma|$ is presented here. The SA is not studied here, since it has nearly the same effect on its performance as PA, which arises from varying its parameters. The effect of varying some geometric parameters (l_2, l_5, w_0, w_4) on $|\Gamma|$ is shown in Fig. 6. In order to analyze the impact of l_2 (vertical spacing between the two arms of folding-shaped strips), the PA is simulated by varying l_2 for the values 0.71, 0.81, and 0.91 mm, while keeping the other parameters unchanged. As observed in Fig. 6(a), as l_2 increases from 0.71 to 0.91 mm, f_r is decreased, and the level of $|\Gamma|$ is also decreased. Also, as shown in Fig. 6(b), with the variation of l_5 (the smallest length of spiral's inner strip) from 0.71 mm to 0.91 mm, f_r decreases with increase in $|\Gamma|$, i.e., more impedance mismatching occurs.

Figures 6(c) and (d) depict the effect of varying w_0 (the length of an extended horizontal arms over feeding region) and w_4 (the horizontal spacing between ending of the mender line and beginning of the spiral) on the reflection coefficient of the proposed PA. Fig. 6(c) exhibits the influence of sweeping w_0 on both f_r and $|\Gamma||_{f_r}$. As noticed, f_r goes to lower frequencies with lower value of $|\Gamma||_{f_r}$ when w_0 is allowed to be varied from 2 to 4 mm. As shown in Fig. 6(d), when the value of w_4 increases from 0.33 to 0.53 mm with step size of 0.1 mm, the resonance frequency shifts towered lower frequency with slightly increasing the level of $|\Gamma|$. It is concluded from this study that varying each one of the parameters does not enhance $|\Gamma|$ of the PA. Therefore, an efficient method is needed to enhance the impedance matching of the designed PA, i.e., to make the level of $|\Gamma||_{f_r}$ less than -15 dB instead of -5.74 dB with the increase of -3 dB impedance bandwidth. To achieve this design requirement, a general optimization methodology will be presented in Section 4.

3. SIMULATED AND MEASURED RESULTS AND DISCUSSIONS

3.1. Simulated Results

The proposed PA and SA are successfully designed and simulated in the previous sections to be conjugate matched to the rectifier impedance of $6 - j170\,\Omega$ at 2.45 GHz. A lumped element of $6\,\Omega$ and capacitor of 0.38212 pF for a reactance of $-j170\,\Omega$ at 2.45 GHz is connected in series with the $50\,\Omega$ discreet port conjugate matched to antenna's input impedance, as shown in Fig. 7.

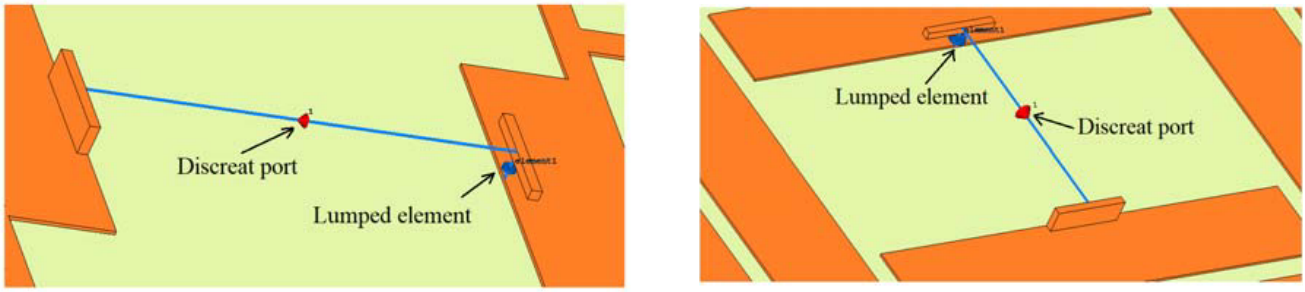

Figure 7. The lumped element (R and C) is connected in series with the $50\,\Omega$ discreet port. (a) PA, (b) SA.

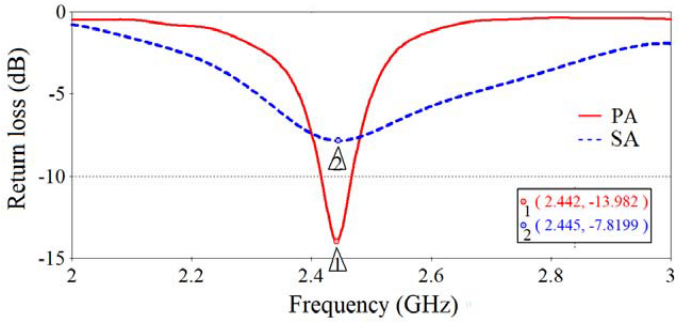

Figure 8. Return loss versus frequency of the proposed antennas (red solid line: PA, blue dash line: SA, black dash line: -10 dB limit.

Figure 8 depicts the return loss characteristics of the proposed antennas when a series lumped element of a resistance $18\,\Omega$ and capacitance 0.3412 pF is connected with a discrete port. As shown in this figure, the two antennas resonate at 2.45 GHz, which are approximately matched to the $50\,\Omega$ of the port. Thus, the designed antennas exhibit good impedance matching that makes them suitably used for energy harvesting application.

3.2. Measured Results and Discussions

The prototypes of the designed antennas are fabricated as shown in Fig. 9. The conventional single ended two-port vector network analyzer (VNA) cannot be used for directly measuring the input impedance and complex reflection coefficient of the proposed antennas since an unbalanced port such as SMA terminal is connected to VNAs. Therefore, an unbalanced port connected to a balanced antenna makes inaccurate measurement for the input impedance due to flow unequal currents in the antenna's terminals.

One of the widely used methods for measuring complex input impedance for balanced antenna is the differential probe method. This method is based on a differential probe fixture which is made from two semi-rigid coaxial cables soldered with each other on the outer conductor as depicted in Fig. 10.

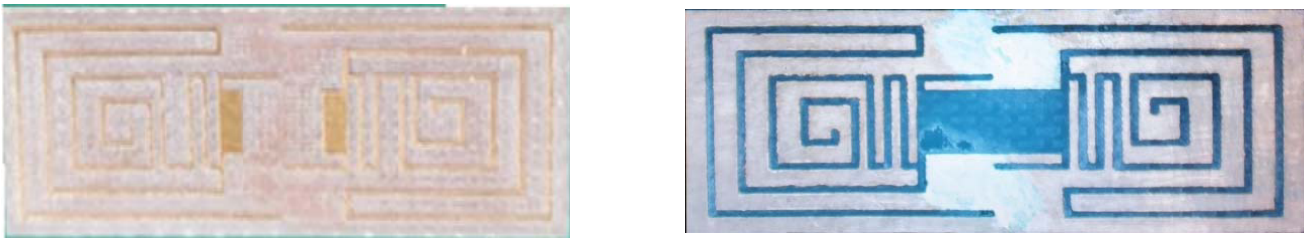

(a) (b)

Figure 9. The photograph of the fabricated antennas. (a) Patch antenna and (b) slot antenna.

Figure 10. Semi-rigid differential probe test fixture for impedance measurement.

(a) (b)

Figure 11. (a) Layout configuration of measurement setup with differential probe, (b) impedance measurement setup with VNA.

The layout configuration of measurement setup with differential probe and impedance measurement setup with VNA are shown in Figs. 11(a) and (b), respectively.

The S-parameters of the manufactured antennas are measured by an Agilent 8719ES VNA. These parameters can be used to calculate the differential input impedance (Z_{in}) as [38]

$$Z_{in} = \frac{2Z_o\left(1 - S_{11}S_{22} + S_{12}S_{21} - S_{12} - S_{21}\right)}{\left(1 - S_{11}\right)\left(1 - S_{22}\right) - S_{12}S_{21}} \tag{4}$$

where Z_o is the characteristic impedance of the connected transmission lines.

Figure 12 shows the simulated and measured complex reflection coefficients $|\Gamma|$ and the real and imaginary parts (R_{in}, X_{in}) of the input impedance Z_{in} of the proposed antennas. The measured and simulated resonance frequencies f_r and $|\Gamma||_{f_r}$, R_{in} and X_{in} at f_r and lower and higher frequencies f_l and f_h, respectively for PA and SA are illustrated in Table 4.

Table 4. Simulated and measured results of the proposed antennas, PA and SA.

Antenna type	Results	f_r (GHz)	$\|\Gamma\|\|_{f_r}$ (dB)	f_l (GHz)	f_h (GHz)	$R_A\|_{f_r}$ (Ω)	$X_A\|_{f_r}$ (Ω)
PA	Simulated	2.445	−5.74	2.426	2.470	18.81	169.92
	Measured	2.440	−6.25	2.402	2.498	37.20	225.60
SA	Simulated	2.449	−8.73 2.429	2.469	13.00	170.74	
	Measured	2.460	−9.65	2.430	> 2.50	36.60	228.82

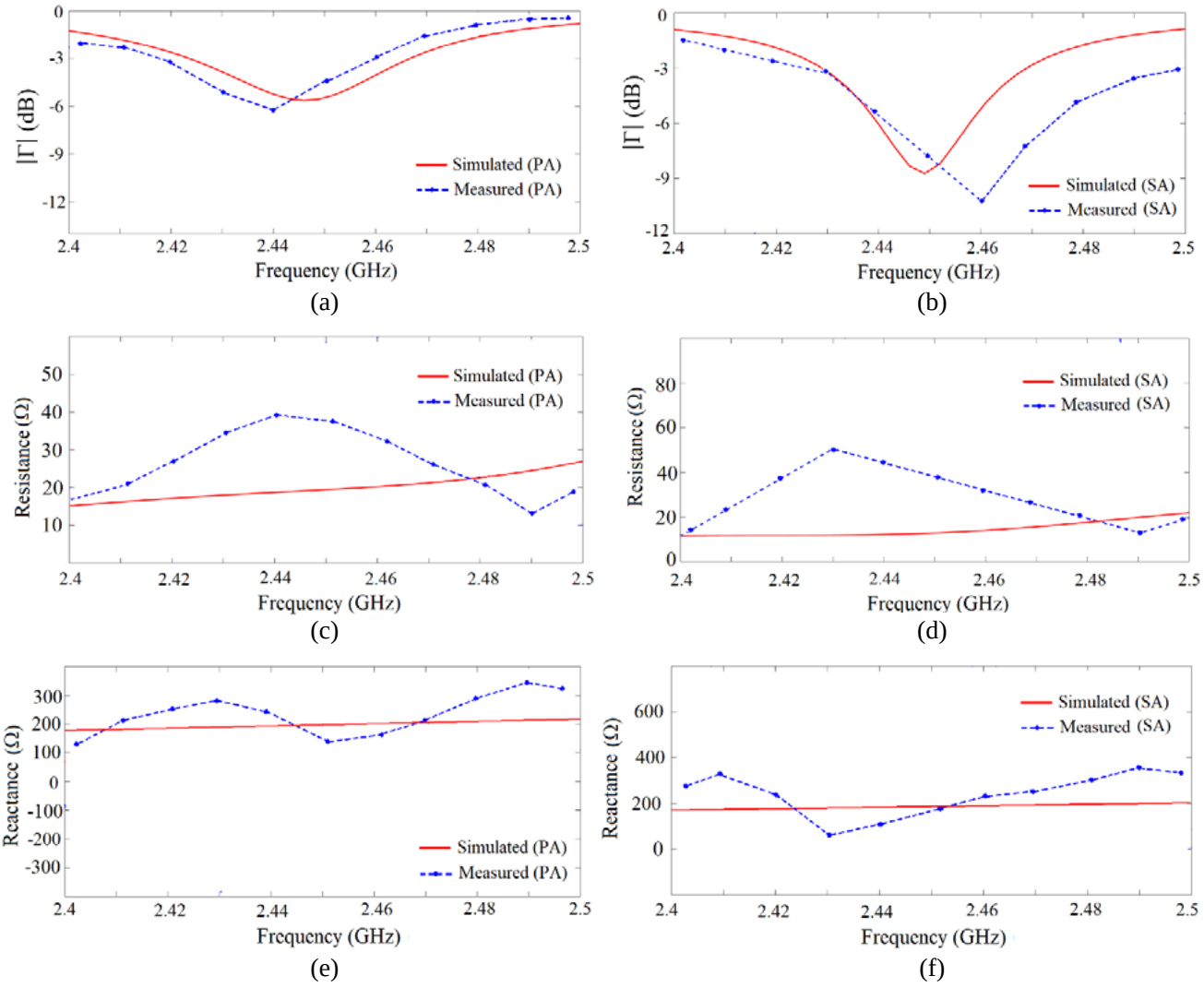

Figure 12. Simulated and measured reflection coefficient (a), (d) $|\Gamma|$, (b), (e) resistance and (c), (f) reactance for the proposed antennas, PA (left) and SA (right), respectively.

It can be noticed that the measured and simulated results are in a good agreement, and the slight variation between the simulated and practical results for patch and slot antennas is due to some factors such as soldering coaxial cable, manufacturing, thickness, dielectric constant, and substrate misalignment.

4. OPTIMIZATION DESIGN METHODOLOGY

This section presents a new optimization design methodology by using a fitness function that takes into account both the desired level of a complex reflection coefficient at given resonance frequencies and the specified lower and higher frequencies constituting the impedance frequency bands. This objective function is applied in designing broadband or multiband antennas having approximately perfect conjugate impedance matching with the impedance of a rectifier suitably used for RFEH application. The particle swarm optimization (PSO) implemented in MATLAB in conjunction with CST simulator is applied as an illustrative example for the designed PA in Section 2.

4.1. Particle Swarm Optimization Implementation

The formulation and implementation of solving the optimization problem for broadband or multiband antennas suitably used for RFEH applications depend on PSO. PSO is adopted in this work as an optimizer algorithm due its interesting features such as global optimization capability, simplified mathematical formulation, and easy implementation for solving complicated optimization problems. Here are the main steps that the antenna designers needed and make them easily utilized for obtaining a feasible solution through the interaction between the PSO algorithm implemented in MATALB and the using of a powerful commercial CST MWS solver. These five steps are described in a way like that presented in [39] and are listed as follows:

1) *Define the Optimization Problem*: This is the first step that determines a proper number of design variables ($x_i,\ i = 1, 2, ..., N_g$) entering the optimization process while suitable design criteria are applied for satisfying the desired specifications. It represents a challenging task by antenna engineers in many applications especially for the problem that requires more than one optimization fitness function.
2) *Define the Solution Space*: As the optimization problem and its design variables have been identified, the next step includes the limitation of the boundaries for each geometric antenna parameter. These boundaries must be made so that it balances between the two requirements, convergence rate and design flexibility. Therefore, a compromise between the above mentioned two requirements must be taken into account by the designer to choose maximum and minimum limits for each one of the N_g optimization parameters, that is, $x_i^{\min} \leq x_i \leq x_i^{\max}$, $i = 1, 2, ..., N_g$.
3) *Define a Fitness Function*: This step is considered the most important among all design steps since a fitness function directly affects the ability of optimization algorithm for getting superior designs. The typical value of a fitness function is described by a single number that represents an optimized performance of a physical system. Therefore, a good fitness function gives an excellent performance characteristic of the optimized design that satisfies the specified requirements. For Electromagnetic (EM) problems such as antennas, a fitness function having clever formulation with simplified mathematical representation and less evaluation computation can rapidly increase the convergence rate of the optimization process.
4) *Initialize Particle Locations and Velocities*: A PSO algorithm is executed by using subsequently steps and initializing each one of the N_p particles randomly throughout its range limit with a uniform distribution. The velocity is also randomly varied with uniformly distributed in the solution space.
5) *Systematically Search the Solution Space*: This final step represents the heart of the optimization process implemented by flying the initialized N_p particles throughout the searching space. It includes the following three sub-steps which are repeated until the convergence criterion limit is satisfied, or the number of iterations is reached:
   a) Evaluate Swarm Fitness: The fitness function is evaluated for all the N_p particles that fly in the swarm region of the solution space.
   b) Update Best Positions: The value of the global best (gBest) and/or the previous best (pBest) locations are given to the current location, if the fitness function is better than one or both.
   c) Update the Particle Position and Velocity: The current location x_{i+1}^k and velocity v_{i+1}^k of a particle k are updated depending on the previous ones x_i^k and v_i^k, respectively according to

the following two formulas:

$$v_{i+1}^k = \omega_i v_i^k + c_1 r_1^k \left(p_i^k - x_i^k\right) + c_2 r_2^k \left(g_i - x_i^k\right) \tag{5a}$$

$$x_{i+1}^k = x_i^k + v_{i+1}^k \tag{5b}$$

where ω_i is the inertial weight at iteration i; p_i^k is the location of the pBest; g_i is the location of the gBest; c_1 and c_2 are cognitive and social weights; and r_1^k and r_2^k are uniformly distributed random variables belonging to the set $(0, 1)$.

4.2. Antenna Optimization Procedure

This section presents a general procedure for applying the aforementioned five design steps throughout the optimization process, as illustrated in the flowchart of Fig. 13. As stated before, a PSO algorithm is implemented in MATLAB for solving the optimization problem, and a CST MWS is adopted as an EM solver for modeling and extracting antenna performance. As noticed, MATLAB and CST MWS programs are responsible for running and executing the blocks shaded by red and blue colors, respectively. Firstly, the first step is described in details in the following section aiming to achieve an optimized patch antenna (OPA) depending on the initialized PA (IPA) designed in Section 2, as an illustrative example. The geometric parameters for IPA are 15 (i.e., $N_g = 15$) which are corresponding to the design variables that entered the optimization process. The details of these design parameters along with their specified boundaries are discussed in the subsequent sections, and this represents the second design step. A new fitness function of the optimization problem which represents the third design step is comprehensively described in the following section.

In the fourth step which represents a first block diagram in Fig. 13, it begins after the optimization process is started. The number of PSO particles is given such that $N_p = 3N_g$, $4N_g$, or $5N_g$ depending on the convergence rate of the design problem to be optimized determined by either reaching the maximum iteration numbers ($N_{\max}$) or specifications have been met. The final fifth step is implemented

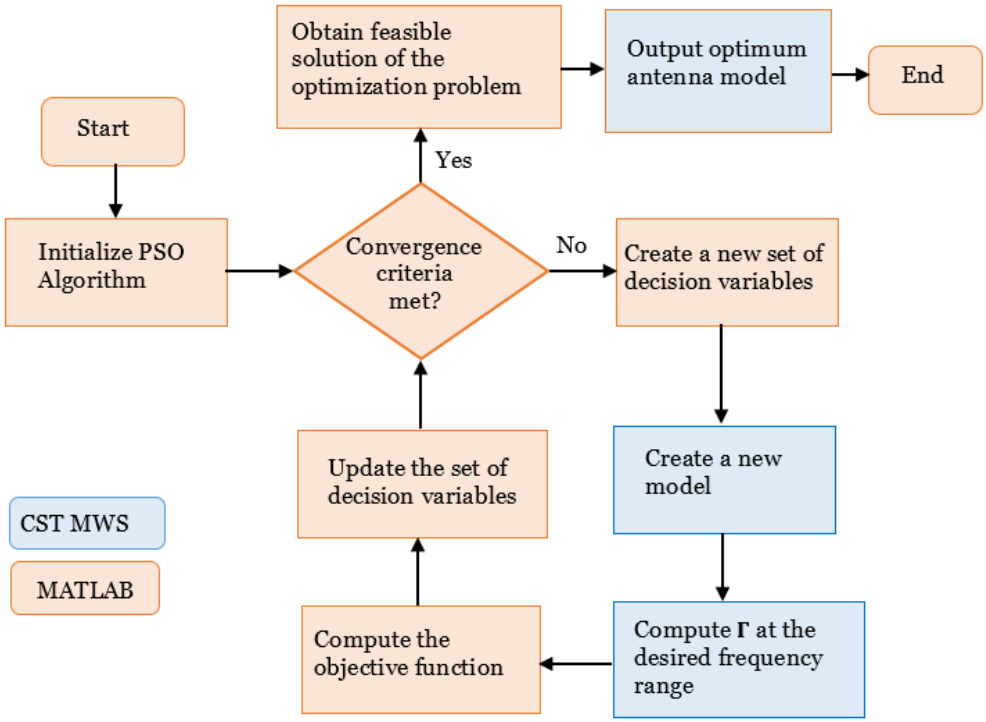

Figure 13. Flowchart to achieve a feasible solution for a given optimization problem by applying the PSO algorithm.

by MATLAB environment to update the design variables by updating the location and velocity of PSO particles, if the criterion is not met. An EM solver (CST MWS) updating the antenna model, i.e., its geometric parameters, depends on the decision variables exported from MATLAB. Then, the complex reflection coefficient at the frequencies of interest is parsed from EM solver to MATLAB for beginning new iteration with updated decision parameters by further computing the objective function. An optimization process is completed when the convergence criteria are met if either maximum iterations reached or desired specification is satisfied. In consequence, the feasible solution of the optimization problem is obtained, and the optimized antenna model is generated with satisfactory performance.

4.3. Optimization Problem for Multiband or Broadband Antennas

The optimization problem for the multiband or broadband antenna is given by

$$\begin{aligned} &\text{Find} \quad \vec{x}^* = \arg\max_x F(\vec{x}, f) \\ &\text{subject to} \quad x \in \mathbb{R}^n \end{aligned} \tag{6}$$

where $\vec{x}$ is a vector of n-design variables defining geometric antenna's parameters, which entered the optimization problem, and the elements of $\vec{x}$ belong to an n-dimensional or the design space, $\mathbb{R}^n$. $F(\vec{x}, f)$ is an objective function that attributes a performance of maximum value to its argument with an optimized candidate solution $\vec{x}^*$. Two sub-objective functions for ith-band, $F_r(\vec{x}, f_r^i)$ and $F_b(\vec{x}, f_l^i, f_h^i)$, constitute the total function $F(\vec{x}, f)$, that is

$$F\left(\vec{x}, f\right) = \sum_i^K c * \min\left\{F_r\left(\vec{x}, f_r^i\right), F_b\left(\vec{x}, f_l^i, f_h^i\right)\right\} - \bar{c} * \Psi \tag{7}$$

where $F_r(\vec{x}, f_r^i)$ is the cost function for the magnitude of a complex reflection coefficient $|\Gamma(\vec{x}, f)|$, which is minimum at a resonance frequency f_r^i for the ith-band and less than a desired criterion limit in dB, $|\Gamma_{rd}|$. $F_b(\vec{x}, f_l^i, f_h^i)$ is the cost function for dealing with the impedance bandwidth for the ith-band by making the values of $|\Gamma(\vec{x}, f)|$ for $f \in (f_{ld}^i, f_{hd}^i)$, where f_{ld}^i and f_{hd}^i are the desired lower and higher frequencies at the ith band, respectively, to be less than $|\Gamma_{bd}|$, the desired criterion limit in dB for $|\Gamma(\vec{x}, f)|$ to define the frequency bands. The symbols c and its complement $\bar{c}$ are binary numbers, which are '0' or '1', and Ψ is a very large value 1×10^{10}, which are introduced for a state when the ith band does not exist, i.e., both f_l^i and f_h^i are not found which results in a worst case, $F(\vec{x}, f) = -\Psi$.

Usually, $\Gamma_{bd} = -10\,\text{dB}$ is used as an upper limit by antenna engineers for matching a conventional antenna with a $50\,\Omega$ transmission lined and $\Gamma_{bd} = -3\,\text{dB}$ for the case for conjugate-matched input impedance of antenna with a complex impedance load. For getting good impedance matching at the K bands, it is preferred to set $\Gamma_{rd} = 3\Gamma_{bd}$. The conventional and perfect $|\Gamma|$ characteristic for operating at the ith frequency band is depicted in Fig. 14.

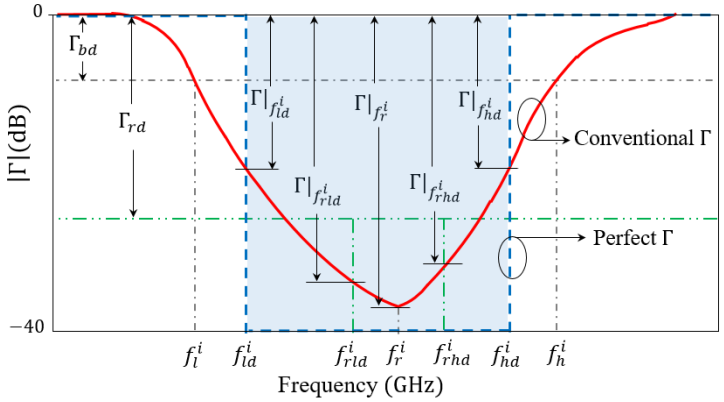

Figure 14. Demonstration of conventional and perfect complex reflection coefficient $|\Gamma|$ for ith band.

As noticed, the aim of the objective function in Eqs. (6) and (7) is to make a designed antenna having an ith band to satisfy the following two requirements:

$$\left|\Gamma\left(\vec{x},f\right)\right|\Big|_{\substack{f_h^i \geq f_{hd}^i,\\ f_l^i \leq f_{ld}^i}} \geq \left|\Gamma_{bd}\right| \quad \text{for } f \in \left(f_l^i, f_h^i\right) \tag{8a}$$

$$\left|\Gamma\left(\vec{x},f\right)\right|\Big|_{\substack{f_r^i \geq f_{rld}^i,\\ f_r^i \leq f_{rhd}^i}} \geq \left|\Gamma_{rd}\right| \quad \text{for } f \in \left(f_{rld}^i, f_{rhd}^i\right), \tag{8b}$$

where f_{rld}^i and f_{rhd}^i are the desired lower and higher resonance frequencies for the ith frequency band, respectively, and $|\Gamma(\vec{x},f)|$ is defined as

$$\left|\Gamma\left(\vec{x},f\right)\right| = 20\log\left[\frac{\left(R_A\left(\vec{x},f\right)-R_L\right)^2+\left(X_A\left(\vec{x},f\right)+X_L\right)^2}{\left(R_A\left(\vec{x},f\right)+R_L\right)^2+\left(X_A\left(\vec{x},f\right)+X_L\right)^2}\right] \text{ (dB)} \tag{9}$$

where $R_A(\vec{x},f)$ and $X_A(\vec{x},f)$ are the real and imaginary parts of antenna impedance $Z_A(\vec{x},f)$ as a function of antennas' geometric parameters and frequency whereas R_L and X_L are the load resistance and reactance, respectively, i.e., $Z_L = R_L + jX_L$, whose fixed values are used at f_r^i.

The cost functions $F_b(\vec{x},f_l^i,f_h^i)$ and $F_r(\vec{x},f_r^i)$ are responsible for satisfying Eqs. (8a) and (8b), respectively. Herein, the detailed mathematical demonstration of $F(\vec{x},f)$ emphasizes that the two aforementioned requirements in Eq. (8) are successfully satisfied by solving the optimization problem given in Eqs. (6) and (7). All auxiliary functions presented here are functions of design variables $\vec{x}$ and frequency f. It is considered that $F_r(\vec{x},f_r^i)$ and $F_b(\vec{x},f_l^i,f_h^i)$ are given by:

$$F_b\left(\vec{x},f_l^i,f_h^i\right) = F_{b1}+F_{b2} \tag{10a}$$

$$F_r\left(\vec{x},f_r^i\right) = F_{r1}+F_{r2} \tag{10b}$$

As noticed in Eq. (10a), two auxiliary functions are introduced. The first one is F_{b1}, and the second is F_{b2} which are accounted for the lower and higher frequencies, f_l^i and f_h^i, respectively, specifying the ith frequency band. Similarly, $F_r(\vec{x},f_r^i)$ in Eq. (10b) is composed of two auxiliary sub-objective functions F_{r1} and F_{r2} which are used to enhance the impedance matching, i.e., antenna input impedance Z_A to be conjugate matched with the load impedance Z_L. Thus, $|\Gamma|$ has the lowest possible value, at a resonance frequency f_r^i by applying these sub-objective functions in the optimization process. The details of forming Eq. (10a) is similar to Eq. (10b) in terms of mathematical equations and concept of operations. Wherefore, it is considered that Eqs. (10a) and (10b) are the same except replacing the subscripts 'b' by 'r', 'l and h' by '1 and 2', and Γ_{bd} by Γ_{rd}, respectively. Thus, the two sub-objective functions F_{b1} and F_{b2} are defined as:

$$F_{b1} = v_{b1}v_{b2} \tag{11a}$$

$$F_{b2} = v_{b1}\overline{v}_{b2} \tag{11b}$$

where

$$\begin{aligned} v_{b1} &= \min\left\{G_l, G_h\right\} \\ v_{b2} &= \max\left\{0, m_{b1}\wedge m_{b2}\right\} \\ \overline{v}_{b2} &= \max\left\{0, \overline{m}_{b1}\vee \overline{m}_{b2}\right\} \end{aligned} \tag{12a}$$

and

$$\begin{aligned} &m_{b1} = u\left(G_l\right), \quad m_{b2} = u\left(G_h\right), \\ &G_l = \left|\Gamma\right|\Big|_{f_{ld}^i} - \left|\Gamma_{bd}\right|, \quad G_h = \left|\Gamma\right|\Big|_{f_{hd}^i} - \left|\Gamma_{bd}\right|, \\ &\overline{G}_l = -G_l, \quad \overline{G}_h = -G_h \end{aligned} \tag{12b}$$

In Eqs. (12a) and (12b), the markers ($\wedge$), ($\vee$), and $\overline{(\ )}$ are AND, OR, and NOT binary logical operators whereas $u(x-a)$ is a unit step function, i.e., its value equals "1" when $x \geq a$ and "0" otherwise. Thus, m_{b1}, m_{b2}, m_{r1}, m_{r2}, v_{b2}, and v_{r2} and their complements $\overline{m}_{b1}$, $\overline{m}_{b2}$, $\overline{m}_{r1}$, $\overline{m}_{r2}$, $\overline{v}_{b2}$, and $\overline{v}_{r2}$ which are binary functions, i.e., they have values either "1" or "0", used for controlling the operation of F_{b1}, F_{b2}, F_{r1}, and F_{r2} during the optimization process. There are sixteen possible values

Table 5. The sixteen cases that may be occurred during optimization process for F_b and F_r depending on the values of $(\pm G_l, \pm G_h)$ and $(\pm G_1, \pm G_2)$. The Case 16$*$ is the optimum case since it is made $F(\vec{x}, f)$ to have a maximum value.

Case	$\pm G_l, \pm G_h$	$\pm G_1, \pm G_2$	$\pm F_b(\vec{x}, f_l^i, f_h^i)$	$\pm F_r(\vec{x}, f_r^i)$
1	$-G_l, -G_h$	$-G_1, -G_2$	$-\min(\lvert G_l\rvert, \lvert G_h\rvert)$	$-\min(\lvert G_1\rvert, \lvert G_2\rvert)$
2	$-G_l, -G_h$	$-G_1, G_2$	$-\min(\lvert G_l\rvert, \lvert G_h\rvert)$	$-G_1$
3	$-G_l, -G_h$	$G_1, -G_2$	$-\min(\lvert G_l\rvert, \lvert G_h\rvert)$	$-G_2$
4	$-G_l, -G_h$	G_1, G_2	$-\min(\lvert G_l\rvert, \lvert G_h\rvert)$	$\min(G_1, G_2)$
5	$-G_l, G_h$	$-G_1, -G_2$	$-G_l$	$-\min(\lvert G_1\rvert, \lvert G_2\rvert)$
6	$-G_l, G_l$	$-G_1, G_2$	$-G_l$	$-G_1$
7	$-G_l, G_l$	$G_1, -G_2$	$-G_l$	$-G_2$
8	$-G_l, G_h$	G_1, G_2	$-G_l$	$\min(G_1, G_2)$
9	$G_l, -G_h$	$-G_1, -G_2$	$-G_h$	$-\min(\lvert G_1\rvert, \lvert G_2\rvert)$
10	$G_l, -G_h$	$-G_1, G_2$	$-G_h$	$-G_1$
11	$G_l, -G_h$	$G_1, -G_2$	$-G_h$	$-G_2$
12	$G_l, -G_h$	G_1, G_2	$-G_h$	$\min(G_1, G_2)$
13	G_l, G_h	$-G_1, -G_2$	$\min(G_l, G_h)$	$-\min(\lvert G_1\rvert, \lvert G_2\rvert)$
14	G_l, G_h	$-G_1, G_2$	$\min(G_l, G_h)$	$-G_1$
15	G_l, G_h	$G_1, -G_2$	$\min(G_l, G_h)$	$-G_2$
16$*$	G_l, G_h	G_1, G_2	$\min(G_l, G_h)$	$\min(G_1, G_2)$

Table 6. The detailed demonstration for calculating the value of the cost function F_b through optimization for the cases 4, 8, 12, and 16$*$ corresponding to the four possibility of (G_l, G_h) and assuming that both (G_l, G_h) have '$+ve$' values.

Case	$\pm G_l, \pm G_h$	m_{b1}, m_{b2}	$\pm v_{b1}$	$\overline{m}_{b1}$, $\overline{m}_{b2}$	v_{b2}	$\overline{v}_{b2}$	$\pm F_{b1}$	$\pm F_{b2}$	$\pm F_b$
4	$-G_l, -G_h$	$0, 0$	$-\min(\lvert G_l\rvert, \lvert G_h\rvert)$	$1, 1$	0	1	0	$-\min(\lvert G_l\rvert, \lvert G_h\rvert)$	$-\min(\lvert G_l\rvert, \lvert G_h\rvert)$
8	$-G_l, G_h$	$0, 1$	$-G_l$	$1, 0$	0	1	0	$-G_l$	$-G_l$
12	$G_l, -G_h$	$1, 0$	$-G_h$	$0, 1$	0	1	0	$-G_h$	$-G_h$
16$*$	G_l, G_h	$1, 1$	$\min(\lvert G_l\rvert, \lvert G_h\rvert)$	$0, 0$	1	0	$\min(\lvert G_l\rvert, \lvert G_h\rvert)$	0	$\min(\lvert G_l\rvert, \lvert G_h\rvert)$

calculated for both the cost functions $F_b(\vec{x}, f_l^i, f_h^i)$ and $F_r(\vec{x}, f_r^i)$ when the optimization is processed depending on values of $|\Gamma||_{f_{ld}^i}$, $|\Gamma||_{f_{hd}^i}$ and $|\Gamma||_{f_{rld}^i}$, $|\Gamma||_{f_{rhd}^i}$ with respect to $|\Gamma_{bd}|$ and $|\Gamma_{rd}|$, respectively. Table 5 illustrates these cases which are denoted as Case 1 to Case 16. In this table, the marker $(*)$ indicates that the total objective function $F(\vec{x}, f)$ is optimum for Case 16 since both F_b and F_r have positive values whereas in the other fifteen cases (Case 1 to Case 15), either F_b or F_r is less than zero, or both have negative values.

The detailed descriptions of eight cases out of these sixteen cases, 4, 8, 12, and 16$*$ (13, 14, 15, 16$*$), for the cost function $F_b(F_r)$ through the optimization are summarized in Tables 6 and 7, respectively. These eight cases are calculated for $F_b(F_r)$ based on the four possibility values of $\pm G_l, \pm G_h$ $(\pm G_1, \pm G_2)$ by assuming that both G_1 and G_2 (G_l and G_h) have positive values or greater than zero.

As sated before, there is an undesirable case that may happen when the ith band is not found, i.e., both f_l^i and f_h^i do not exist. This unwanted case can be taken into consideration as seen in the optimization function in Eq. (7) by using Ψ as a very large value 1×10^{10} and two control functions c

Table 7. The detailed demonstration for calculating the value of the cost function F_r through optimization for the cases 12, 13, 14, and 16∗ corresponding to the four possibility of (G_1, G_2) and assuming that both (G_l, G_h) have '$+ve$' values.

Case	$\pm G_1, \pm G_2$	m_{r1}, m_{r2}	$\pm v_{r1}$	$\overline{m}_{r1}$, $\overline{m}_{r2}$	v_{r2}	$\overline{v}_{r2}$	$\pm F_{r1}$	$\pm F_{r2}$	$\pm F_r$
13	$-G_1, -G_2$	$0, 0$	$-\min(\lvert G_1\rvert, \lvert G_2\rvert)$	$1, 1$	0	1	0	$-\min(\lvert G_1\rvert, \lvert G_2\rvert)$	$-\min(\lvert G_1\rvert, \lvert G_2\rvert)$
14	$-G_1, G_2$	$0, 1$	$-G_1$	$1, 0$	0	1	0	$-G_1$	$-G_1$
15	$G_1, -G_2$	$1, 0$	$-G_2$	$0, 1$	0	1	0	$-G_2$	$-G_2$
16∗	G_1, G_2	$1, 1$	$\min(\lvert G_1\rvert, \lvert G_2\rvert)$	$0, 0$	1	0	$\min(\lvert G_1\rvert, \lvert G_2\rvert)$	0	$\min(\lvert G_1\rvert, \lvert G_2\rvert)$

and its complement $\overline{c}$ which are binary numbers, i.e., they have a value of '0' or '1', and may be written as

$$c = u\left(|\Gamma_{\min}|\,|_{f=f_r^i} - |\Gamma_{bd}|\right), \quad f \in \left(f_{ld}^i, f_{hd}^i\right) \tag{13a}$$

$$\overline{c} = u\left(-|\Gamma_{\min}|\,|_{f=f_r^i} + |\Gamma_{bd}|\right), \quad f \in \left(f_{ld}^i, f_{hd}^i\right) \tag{13b}$$

In Eq. (13a) and (13b), $u(\,)$ is a unit step function, and c is at logic '1' when the minimum value of $|\Gamma|$ at the resonance frequency f_r^i, i.e., $|\Gamma_{\min}||_{f=f_r^i}$, is greater than $|\Gamma_{bd}|$; otherwise, c has a value of '0'. On the other hand, $\overline{c}$ is a complement of c ($\overline{c} = -c$) or ($\overline{c} = \text{NOT}\, c$). This unwanted case, which makes $F(\vec{x}, f) = -\Psi$, occurs if Eq. (8b) is not satisfied, i.e., the desired ith band with an appropriate level of impedance matching is not achieved. This unwanted case is called a Case 0.

As noticed from Table 7, the optimum value of $F_r(\vec{x}, f_r^i)$ is corresponding to Case 16∗. Thus, the maximum positive value of F_r is obtained in this case for both the values of G_1 and G_2 which are greater than or equal to zero, i.e., they have positive values. On the other hand, in cases 13–15, $F_r(\vec{x}, f_r^i)$ has a negative value since either G_1 or G_2 or both have negative values. In summary, the proposed objective function described in details previously is eligible for using subsequently in this work for enhancing the performance of the antenna designed in Section 2. This enhancement includes both the degree of conjugate-matching of the antenna input impedance to the rectifier impedance at a desired resonance frequency, 2.45 GHz (ISM band), and widening the band of designed antenna to operate in the specified band (2.4–2.5 GHz).

4.4. Design of an Optimized Antenna

In this section, a PA designed in Section 2 is considered here as an initial design, namely IPA to be optimized by the optimization procedure described earlier. The aim is to achieve an optimized PA (OPA) having good impedance matching (i.e., $Z_A = Z_L^*$) at the desired resonance frequency f_{rd} with broadband characteristic specified by the lower and higher frequencies f_{ld} and f_{hd}, respectively. Z_L herein represents an impedance of a typical rectifier (HSMS-286C) with a value of $6 - j170\,\Omega$ at $f_{rd} = 2.45$ GHz. Tables 8, 9, and 10 summarize the desired specifications, ranges of design parameters that entered optimization process, and dimensions of the unchanged geometrical parameters, respectively.

Table 8. The desired frequencies constituting the desired band that used in the design optimization methodology.

Desired parameter	f_{ld}	f_{hd}	f_{rd}	f_{rld}	f_{rhd}
Value (GHz)	2.40	2.50	2.45	2.445	2.455

As discussed in Section 2, the design parameter (t) is considered as an independent geometric parameter on which the remaining 15 ($w_1, ..., w_{10}$ and $l_1, ..., l_5$) depend and are called the dependent parameters. Also, as indicated in Section 2, the overall dimensions of the IPA are characterized by

Table 9. Antenna geometric parameters unvaried during optimization.

Parameter	t	w_0	a	b	h_{sub}
Value (mm)	0.3	3.0	3.0	1.0	0.8

Table 10. Ranges of the dependent geometric parameters used for achieving OPA.

Parameter	Range (mm)	Parameter	Range (mm)
w_1	$0.3 \sim 1.8$	w_9	$0.3 \sim 1.8$
w_2	$0.3 \sim 1.8$	w_{10}	$0.3 \sim 1.8$
w_3	$0.3 \sim 1.8$	l_1	$0.3 \sim 2.4$
w_4	$0.3 \sim 1.8$	l_2	$0.3 \sim 2.4$
w_5	$0.3 \sim 1.8$	l_3	$0.3 \sim 2.4$
w_6	$0.3 \sim 1.8$	l_4	$1.2 \sim 2.4$
w_7	$0.3 \sim 1.8$	l_5	$1.2 \sim 2.4$
w_8	$0.3 \sim 1.8$		

$W_{sub} \times L_{sub}$ which depend on the dependent and independent parameters. Thus, OPA is achieved with desired performance as a result by applying the proposed fitness function and using the optimization model in Fig. 13.

As described in Fig. 13, CST MWS is used for extracting $|\Gamma|$ at the frequency of interest (2.2–2.8 GHz), and PSO implemented in MALAB simulation tool is adopted as an optimization algorithm. The criterion used for stopping the optimization process is either that the maximum iterations is reached ($N_{\max} = 100$) or that the value of fitness function is greater than zero, i.e., $F(\vec{x}, f) \geq 0$. In order to achieve a good convergence rate with an acceptable time processing, the number of PSO particles N_p used is 60, i.e., $N_p = 4N_g$, where $N_g = 15$ is the number of geometric PA dimensions that enter the optimization process.

5. RESULTS AND DISCUSSIONS

This section presents the simulated and measured results of the optimized antenna, i.e., OPA. These results include the simulated and measured complex reflection coefficients $|\Gamma|$, the antenna input impedance as a function of frequency, simulated far-field radiation characteristics, radiation patterns, and realized gain and efficiency.

5.1. Optimized Antenna Geometric Dimensions and Performance

Figure 15 illustrates the final geometry of OPA, and Table 11 lists the values of the optimized dimensions achieved as a result of using the optimization process described in the previous sections. These values represent the feasible solution for the broadband OPA. Figs. 16(a) and (b) show the complex reflection coefficient $|\Gamma|$ characteristics and the real R_A and imaginary X_A parts of antenna input impedance $Z_A = R_A + jX_A$ for the initial and optimized patch antennas (IPA) and (OPA), respectively.

From the depicted plots in Fig. 16(a), one can observe that OPA has good $|\Gamma|$ performance in comparison with IPA for both the level of impedance matching and frequency band. Also, as shown in Fig. 16(b), OPA has good conjugate match compared to IPA with $Z_L = 6 - j170\,\Omega$ at 2.45 GHz, i.e., $Z_A = 8.619 + j170.690\,\Omega$ and $18.765 + j169.800\,\Omega$, respectively. Table 12 summarizes the final values of the design parameters used for computing the fitness function (F) when the optimization process is stopped for reaching the specified maximum number of iterations, $N_{\max} = 100$. As noticed, both values of G_1 and G_2 are greater than zero whereas both the values of G_l and G_h are less than zero. These

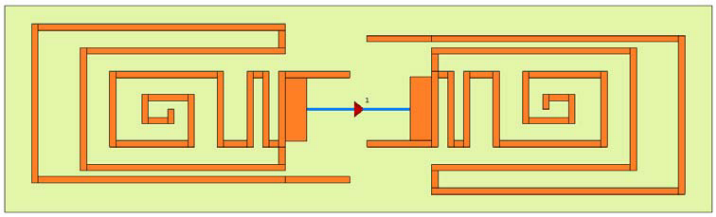

Figure 15. The optimized patch antenna (OPA).

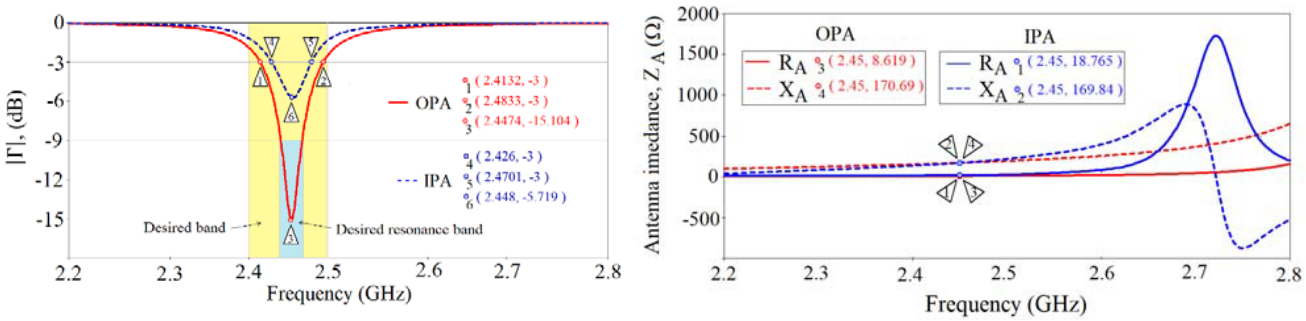

Figure 16. (a) The complex reflection coefficient $|\Gamma|$ characteristics and (b) the real and imaginary parts of input impedance for the proposed initial and optimized patch antennas (IPA) and (OPA), respectively.

Table 11. Feasible solution of the OPA antenna achieved by the optimization process described in Fig. 13. Also, IPA geometric parameters are listed for comparison.

Parameter	Value (mm)		Parameter	Value (mm)	
	OPA	IPA		OPA	IPA
W_{sub}	32.87	27.36	w_6	0.9	1.08
L_{sub}	9.68	10.52	w_7	1.2	1.08
h_{sub}	0.8	0.80	w_8	1.06	1.08
a	3.0	1.0	w_9	1.95	1.08
b	1.0	3.0	w_{10}	1.26	1.08
w_0	3.0	3.0	l_1	1.122	0.81
w_1	0.45	0.43	l_2	0.54	0.81
w_2	0.43	0.43	l_3	0.81	0.81
w_3	1.08	0.43	l_4	0.78	0.81
w_4	1.065	1.08	l_5	0.39	0.81
w_5	0.64	0.57			

values represent Case 4 that is illustrated in Table 5. Also, it is noticed from Table 6 that $F_r = 2.69$ and $F_b = -1.311$ which produces $F = -1.311$ by using a minimum value of them.

It is concluded from Fig. 16 and Table 12 that F is close to the optimum value ($F \geq 0$), i.e., Case 16$*$ in Table 5. Moreover, the desired resonance frequency $f_{rd} = 2.45\,\text{GHz}$ is within the two desired lower and higher resonance frequencies $f_{rld} = 2.445\,\text{GHz}$ and $f_{rhd} = 2.455\,\text{GHz}$, respectively. Also, the lower and higher frequencies $f_l = 2.413\,\text{GHz}$ and $f_h = 2.483\,\text{GHz}$ are close to the desired lower and higher frequencies $f_{ld} = 2.4\,\text{GHz}$ and $f_{hd} = 2.5\,\text{GHz}$, respectively. Thus, the proposed fitness function

Table 12. The values of the design parameters that used to calculate the fitness function (F) after reaching a maximum number of iterations ($N_{\max} = 100$).

Design parameter	f_l	f_{ld}	f_h	f_{hd}	f_{rld}	f_r	f_{rhd}
Value (GHz)	2.413	2.4	2.483	2.5	2.445	2.447	2.455
Design parameter	$\|\Gamma\|\|_{f_l}$	$\|\Gamma\|\|_{f_{ld}}$	$\|\Gamma\|\|_{f_h}$	$\|\Gamma\|\|_{f_{hd}}$	$\|\Gamma\|\|_{f_{rld}}$	$\|\Gamma\|\|_{f_{rd}}$	$\|\Gamma\|\|_{f_{rhd}}$
Value (dB)	3	1.837	3	1.689	14.395	15.104	11.690
Design parameter	G_l	G_h	F_b	G_1	G_2	F_r	F
Value (dB)	−1.163	−1.311	−1.311	5.395	2.690	2.690	−1.311

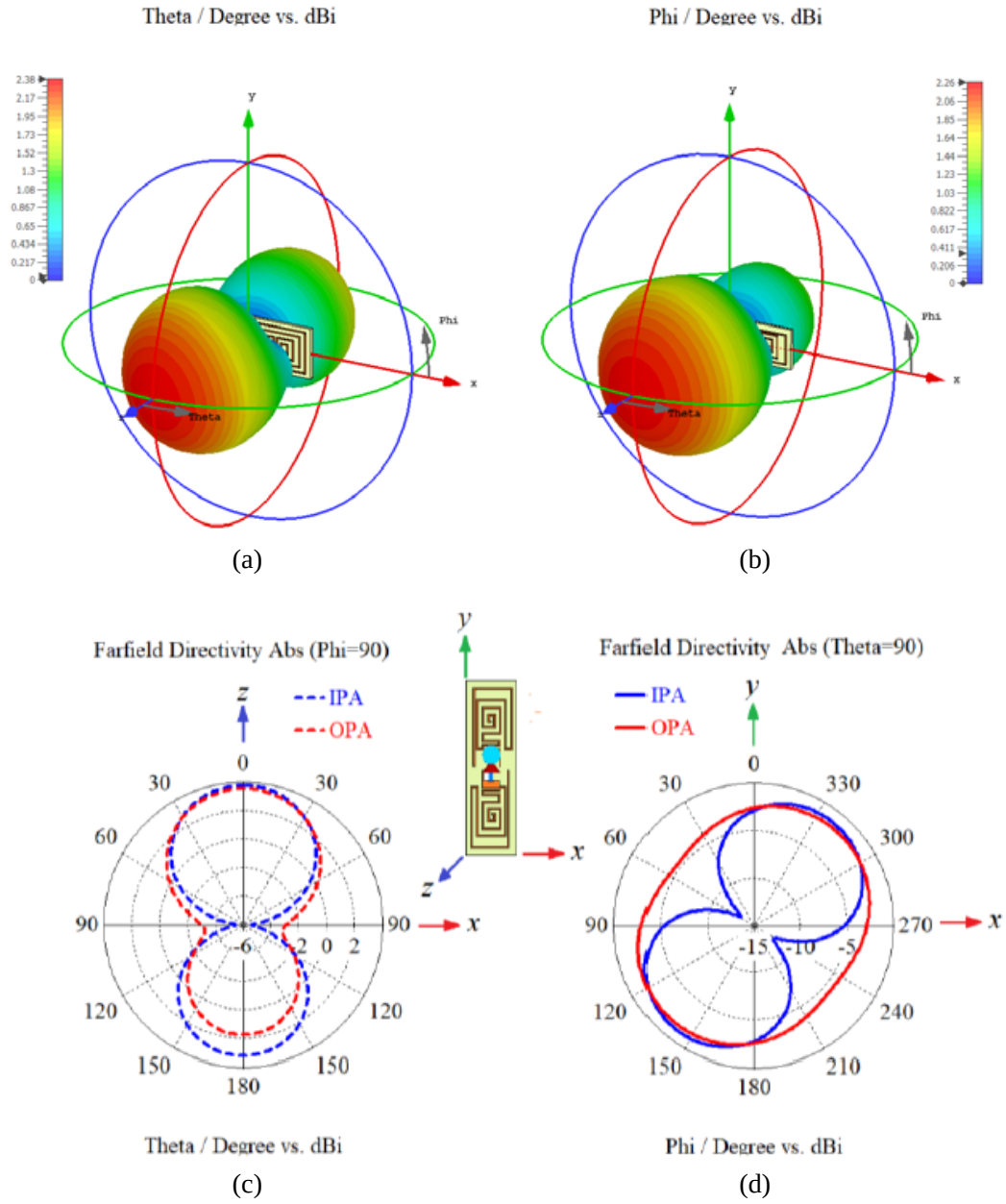

Figure 17. The simulated 3D radiation pattern at 2.45 GHz for (a) IPA and (b) OPA. The 2D polar plot for IPA and OPA, (c) E-plane and (d) H-plane.

presented in this work is successfully finding the optimum feasible solution of OPA suitable for RFEH applications.

Figure 17 shows the 3D and 2D radiation patterns of the proposed IPA and OPA at 2.45 GHz in both E- and H-planes. As noticed in Figs. 17(a) and (b), OPA has more radiation in its front side whereas nearly equal radiation in the front and back sides is exhibited by IPA. Also, as observed in Figs. 17(c) and (d), OPA has nearly omnidirectional radiation in H-plane and approximately figure of eight in E-plane. Thus, OPA is more efficient than IPA for omnidirectional radiation characteristic which is desired for RFEH applications. The radiation efficiency and gain of the proposed antennas are exhibited in Figs. 18(a) and (b), respectively. As observed, the two antennas have low efficiency and gain performance at the frequencies of interest (2.2–2.8 GHz). This drawback in radiation capability may happen due to the miniaturized sizes of these antennas, cancelation in the distributed currents at their surfaces, or more losses produced from the FR4 substrate. Anyway, OPA is 1 dB larger in gain and 50% lower in efficiency than IPA at 2.45 GHz.

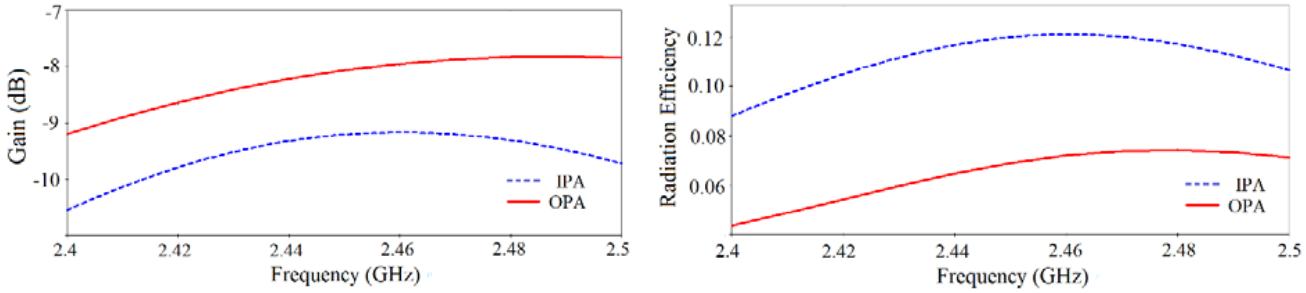

Figure 18. Comparison of antenna performances between the proposed antennas, IPA and OPA. (a) Realized gain. (b) Radiation efficiency.

5.2. Measured Results and Discussions

The fabricated OPA is depicted in Fig. 19(a), and Fig. 19(b) shows the differential probe test fixture used for measuring the input impedance Z_{in} for the OPA. As described in Section 2, Z_{in} is defined by Eq. (4) based on the measurement S-parameters when a two-port test cable of the differential probe is connected to VNA. Fig. 20 shows the measurement S-parameters for OPA.

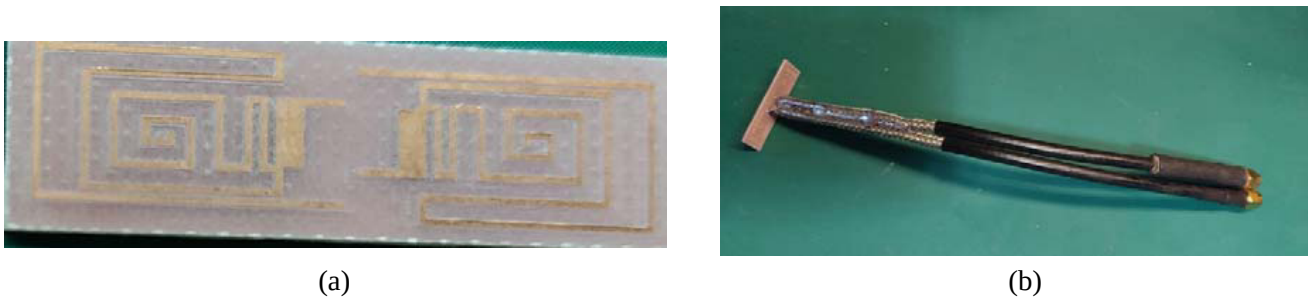

Figure 19. (a) A fabricated prototype of OPA. (b) Simi-rigid differential probe test fixture for impedance measurement of OPA.

Figure 21 shows the measurement and simulated complex reflection coefficient $|\Gamma|$ and the real and imaginary parts, R_{in} and X_{in}, respectively for Z_{in}. Table 13 lists the simulated and measured results for R_{in}, X_{in} besides $|\Gamma|$ at the resonance frequency f_r and the -3 dB impedance bandwidth defined by the lower and higher frequencies f_l and f_h, respectively. It is clear from Table 13 that the simulated and measured results are close to each other, and a little difference between them can be caused by fabrication tolerances and errors attributed from extended port of the differential port.

Table 13. Simulated and measured results of the proposed antenna, OPA.

Results	f_r (GHz)	$\|\Gamma\|_{f_r}$ (dB)	f_l (GHz)	f_h (GHz)	$R_A\|_{f_r}$ (Ω)	$X_A\|_{f_r}$ (Ω)
Simulated	2.447	−15.107	2.413	2.483	8.619	170.69
Measured	2.470	−12.690	2.402	2.500	15.85	215.62

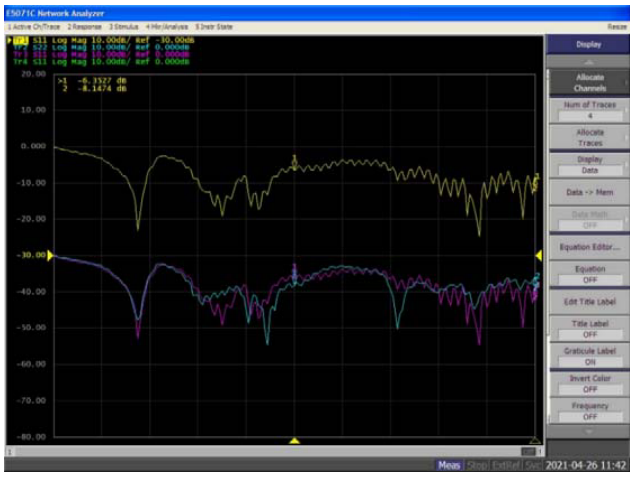

Figure 20. The measured S-parameters for OPA.

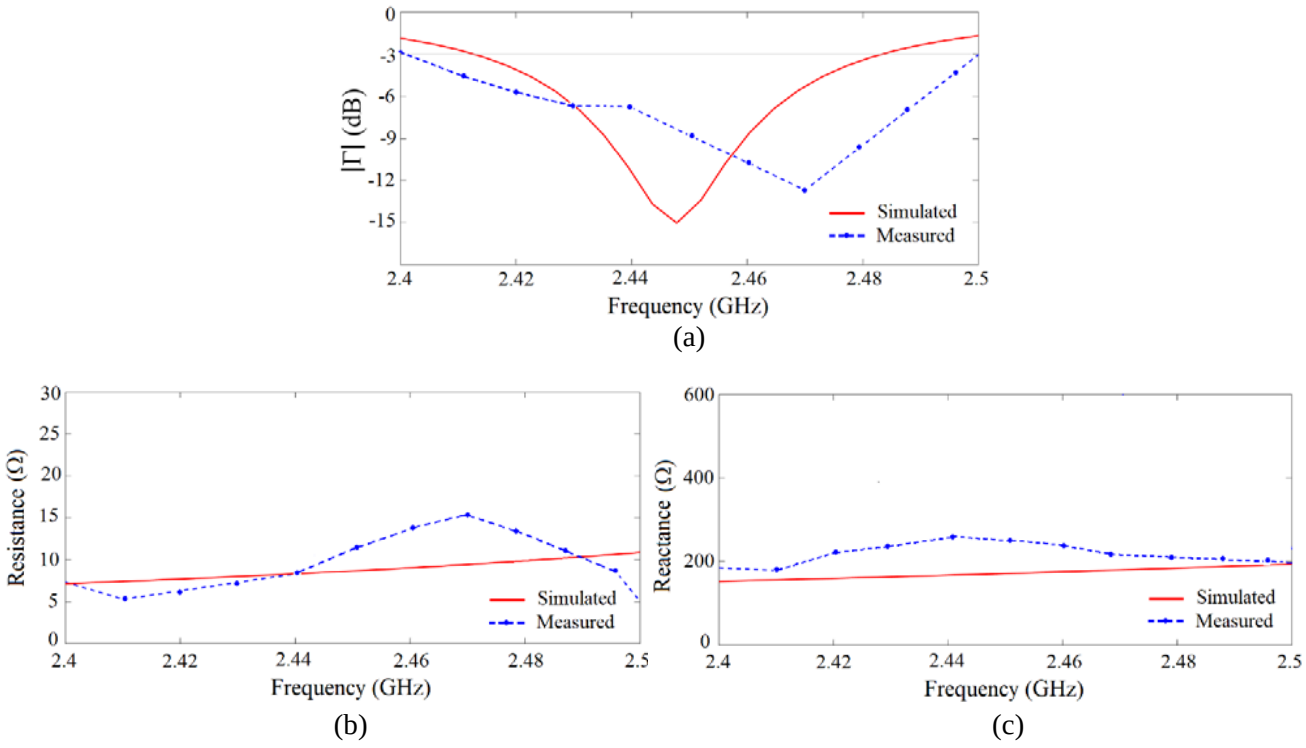

Figure 21. Simulated and measured reflection coefficient (a) $|\Gamma|$, (b) resistance and (c) reactance for the proposed OPA.

Table 14. Performance comparison of the proposed antenna with those in the literature.

Ref.	Antenna type	Frequency band (GHz)	Substrate, Dielectric Constant, Thickness (mm)	Physical size ($W_{sub} \times L_{sub}$)	Use of impedance matching	% Reduction in size
[4]	Patch and Quasi-Yagi antenna	2.45	FR4, $\epsilon_r = 4.4$ $h_{sub} = 0.8$	$70 \times 60\,\text{mm}^2$	No	92.5
[5]	Octagonal antenna	2.2	RT/Doroid 5880 Rogers $\epsilon_r = 3.9, h_{sub} = 1.6$	$71 \times 71\,\text{mm}^2$	No	93.7
[18]	Vivaldi antenna	2.45	FR4, $\epsilon_r = 3.9$ $h_{sub} = 1.6$	$76.8 \times 76\,\text{mm}^2$	Yes	94.6
[19]	Rectangular strip-loop	2.45	Transparent Plexiglas $\epsilon_r = 4.3, h_{sub} = 2$	$100 \times 100\,\text{mm}^2$	yes	96.8
[20]	Slotted-star shaped slot antenna	2.45	F4B-2, $\epsilon_r = 2.65$ $h_{sub} = 1.5$	$135 \times 93\,\text{mm}^2$	yes	97.5
[21]	Star-shaped patch antenna	2.45	RT/Duroid 6002, $\epsilon_r = 2.94$ $h_{sub} = 25$	$110 \times 90\,\text{mm}^2$	No	96.8
This work	**Meander, spiral and double-folded patch antenna**	**2.45**	**FR4, $\epsilon_r = 4.3$ $h_{sub} = 0.8$**	**$32.8 \times 9.6\,\text{mm}^2$**	**No**	**-**

5.3. Comparison with Other Works

The comparison among the proposed OPA and other reported published antennas in literature in terms of dimension, antenna type, substrate used, frequency band, and use of matching circuit is summarized in Table 14. It is clear from this table that the proposed antenna has a miniaturized dimension compared with all the reported antennas. Also, this work presents an efficient general optimization procedure for designing antennas that satisfy the specified requirements needed in RFEH applications without using impedance matching networks.

6. CONCLUSION

A new general optimization methodology is presented in this work for designing broadband or multiband antennas suitably used for RFEH applications. A fitness function is proposed for the first time to successfully deal with both the level of the complex reflection coefficient at the desired resonance frequencies and the lower and higher frequencies of the frequency bands. To demonstrate the effectiveness of this optimization approach, a broadband optimized patch antenna (OPA) is optimized from its counterpart initialized PA (IPA) to operate at the desired 2.45 GHz WLAN band (2.4–2.5 GHz). The OPA is obtained at the end of optimization, and it has more than -15 dB of Γ compared with $\Gamma = -5.74$ dB for IPA at 2.45 GHz. Moreover, OPA has nearly more than 40% of -3 dB-Γ impedance bandwidth ranging from 2.41 to 2.49 GHz in comparison with IPA counterpart which operates in 2.43–2.47 GHz band. The OPA is fabricated on an FR4 substrate with an overall size of $32.8 \times 9.7 \times 0.8\,\text{mm}^3$, and the measured results in terms of -3 dB-Γ impedance bandwidth agree well with the simulated ones which makes it an appropriate candidate as an antenna for RF EH systems.

REFERENCES

1. Ran, L. G., H. K. Cha, and W. T. Park, "RF power harvesting: A review on designing methodologies and applications," *Micro. and Nano Syst. Lett.*, Vol. 5, 14, 2017.
2. Sleebi, K., D. Deepti, and Nasimuddin, "RF energy harvesting systems: An overview and design issues," *Int. J. RF Microw. Comput. Aided Eng.*, Vol. 29, No. 1, 1–15, 2018.
3. Wagih, M., A. S. Weddell, and S. Beeby, "Rectennas for radio-frequency energy harvesting and wireless power transfer: A review of antenna design [antenna applications corner]," *IEEE Antennas and Propagation Magazine*, Vol. 62, No. 5, 95–107, Oct. 2020, doi: 10.1109/MAP.2020.3012872.
4. Chen, Y. and C. Chiu, "Maximum achievable power conversion efficiency obtained through an optimized rectenna structure for RF energy harvesting," *IEEE Trans. Antennas Propag.*, Vol. 65, No. 5, 2305–2317, May 2017, doi: 10.1109/TAP.2017.2682228.
5. Almoneef, S., "Design of a rectenna array without a matching network," *IEEE Access*, Vol. 8, 109071–109079, 2020, doi: 10.1109/ACCES.2020.3001903.
6. Song, C., et al., "Matching network elimination in broadband rectennas for high-efficiency wireless power transfer and energy harvestin," *IEEE Transactions on Industrial Electronics*, Vol. 64, No. 5, 3950–3961, May 2017, doi: 10.1109/TIE.2016.2645505.
7. Sabhan, D., V. J. Nesamoni, and J. Thangappan, "An efficient 2.45 GHz spiral rectenna without a matching circuit for RF energy harvesting," *Wireless Personal Communications*, Vol. 119, 713–726, 2021.
8. Jing, J., J. Pang, S. Wang, Z. Qiu, and C. Liu, "A compact hollowed-out loop rectenna without matching network for wireless sensor applications," *Int. J. RF Microw. Comput. Aided Eng.*, e22417, 2020.
9. Zeng, M., A. S. Andrenko, X. Liu, Z. Li, and H.-Z. Tan, "A compact fractal loop rectenna for RF energy harvesting," *IEEE Antennas Wireless Propag. Lett.*, Vol. 16, 2424–2427, 2017.
10. Wagih, M. , A. S. Weddell, and S. Beeby, "Meshed high-impedance matching network-free rectenna optimized for additive manufacturing," *IEEE Open Journal of Antennas and Propagation*, Vol. 1, 615–626, 2020, doi: 10.1109/OJA.2020.3038001.
11. Visser, H., S. Keyrouz, and A. Smolders, "Optimized rectenna design," *Wireless Power Transfer*, Vol. 2, No. 1, 44–50, 2015, doi: 1.1017/wpt.2014.14.
12. Sun, H., Y.-X. Guo, M. He, and Z. Zhong, "Design of a high-efficiency 2.45-GHz rectenna for low-input-power energy harvesting," *IEEE Antennas Wireless Propag. Lett.*, Vol. 11, 929–932, 2012.
13. Hagerty, J. A., F. B. Helmbrecht, W. H. McCalpin, R. Zane, and Z. B. Popovic, "Recycling ambient microwave energy with broad-band rectenna arrays," *IEEE Trans. Microw. Theory Techn.*, Vol. 52, No. 3, 1014–1024, Mar. 2004.
14. De Long, B. J., A. Kiourti, and J. L. Volakis, "A radiating near-field patch rectenna for wireless power transfer to medical implants at 2.4 GHz," *IEEE Journal of Electromagnetics, RF and Microwaves in Medicine and Biology*, Vol. 2, No. 1, 64–69, Mar. 2018, doi: 10.1109/JER.2018.2815905.
15. Shen, S., C. Chiu, and R. D. Murch, "A dual-port triple-band l-probe microstrip patch rectenna for ambient RF energy harvesting," *IEEE Antennas Wireless Propag. Lett.*, Vol. 16, 3071–3074, 2017, doi: 10.1109/LAW.2017.2761397.
16. Shi, Y., Y. Fan, Y. Li, L. Yang, and M. Wang, "An efficient broadband slotted rectenna for wireless power transfer at LTE band," *IEEE Trans. Antennas Propag.*, Vol. 67, No. 2, 814–822, Feb. 2019, doi: 10.1109/TAP.2018.2882632.
17. Nie, M., X. Yang, G. Tan, and B. Han, "A compact 2.45-GHz broadband rectenna using grounded coplanar waveguid," *IEEE Antennas Wireless Propag. Lett.*, Vol. 14, 9860–989, Dec. 2015, doi: 10.1109/LAW.2015.2388789.
18. Hassan, N., Z. Zakaria, Y. W. Sam, and I. N. M. Hanapiah, "Design of dual-band micro strip patch antenna with right-angle triangular aperture slot for energy transfer application," *Wiley RF and Microwave Computer-Aided Engineering*, e21666, 2018.

19. Mohd Noor, F. S., Z. Zakaria, H. Lago, and M. A. Meor Said, "Dual-band aperture-coupled rectenna for radio frequency energy harvesting," *Int. J. RF Microw. Comput. Aided Eng.*, Vol. 29, No. 1, e21651, 2019.
20. Bhatt, K., S. Kumar, P. Kumar, and C. C. Tripathi, "Highly efficient 2.4 and 5.8 GHz dual-band rectenna for energy harvesting applications," *IEEE Antennas Wireless Propag. Lett.*, Vol. 18, No. 12, 2637–2641, Dec. 2019, doi: 10.1109/LAW.2019.2946911.
21. Sun, H., Y.-X. Guo, M. He, and Z. Zhong, "Design of a high-efficiency 2.45-GHz rectenna for low-input-power energy harvesting," *IEEE Antennas Wireless Propag. Lett.*, Vol. 11, 929–932, 2012.
22. Boursianis, A. D., et al., "Multiband patch antenna design using nature-inspired optimization method," *IEEE Open Journal of Antennas and Propagation*, Vol. 2, 151–162, 2021, doi: 10.1109/OJA.2020.3048495.
23. Ahn, C.-H. and S. Oh, "High gain pentagonal loop rectifying antenna," *Microw. Opt. Technol. Lett.*, Vol. 60, 1075–1079, 2018.
24. Travassos, X. L., D. A. G. Vieira, and A. C. Lisbo, "Antenna optimization using multiobjective algorithms," *ISRN Communications and Networking*, Vol. 2012, 2012.
25. Kaur, G., M. Rattan, and C. Jain, "Optimization of swastika slotted fractal antenna using genetic algorithm and bat algorithm for S-band utilities," *Wireless Personal Communications*, Vol. 97, No. 1, 95–107, 2017.
26. Kaur, G., M. Ratta, and C. Jain, "Design and optimization of psi (ψ) slotted fractal antenna using ANN and GA for multiband applications," *Wireless Personal Communications*, Vol. 97, No. 3, 4573–4585, 2017.
27. Jayasinghe, J. W., J. Anguera, and D. N. Uduwawala, "A simple design of multi band microstrip patch antennas robust to fabrication tolerances for GSM, UMT, LTE, and Bluetooth applications by using genetic algorithm optimization," *Progress In Electromagnetics Research M*, Vol. 27, 255–269, 2012.
28. Jabar, A. A. S. A. and D. K. Naji, "Optimization design methodology of miniaturized five-band antenna for RFID, GSM, and WiMAX applications," *Progress In Electromagnetics Research B*, Vol. 83, 177–201, 2019.
29. Jin, N. and Y. Rahmat-Samii, "Hybrid real-binary particle swarm optimization (HPSO) in engineering electromagnetics," *IEEE Trans. Antennas Propag.*, Vol. 58, No. 12, 3786–3794, 2010.
30. Jin, N. and Y. Rahmat-Samii, "Advances in particle swarm optimization for antenna designs: Real-number, binar, single-objective and multiobjective implementation," *IEEE Tran. Antennas Propag.*, Vol. 55, No. 3, 556–567, 2007.
31. Choudhury, B., S. Manickam, and R. M. Jha, "Particle swarm optimization for multiband metamaterial fractal antenna," *Journal of Optimization*, 2013.
32. Sun, L.-L., J.-T. Hu, K.-Y. Hu, M.-W. He, and H.-N. Chen, "Multi-species particle swarms optimization based on orthogonal learning and its application for optimal design of a butterfly shaped patch antenna," *J. Cent. South Univ.*, Vol. 23, No. 8, 2048–2062, 2016.
33. Tang, M.-C., X. Chen, M. Li, and R. Ziolkowski, "Particle swarm optimized, 3D-printed, wideband, compact hemispherical antenna," *IEEE Antennas Wireless Propag. Lett.*, Vol. 17, N. 11, 2031–2035, 2018.
34. Martinez-Fernandez, J., J. M. Gil, and J. Zapata, "Ultrawideband optimized profile monopole antenna by means of simulated annealing algorithm and the finite element method," *IEEE Trans. Antennas Propag.*, Vol. 55, No. 6, 1826–1832, 2007.
35. Dastranj, A., "Optimization of a printed UWB antenna: Application of the invasive weed optimization algorithm in antenna design," *IEEE Antennas and Propagation Magazine*, Vol. 59, No. 1, 48–57, 2017.
36. Monavar, F. M., N. Komjani, and P. Mousavi, "Application of invasive weed optimization to design a broadband patch antenna with symmetric radiation pattern," *IEEE Antennas Wireless Propag. Lett.*, Vol. 10, 1369–1372, 2011.

37. Karimkashi, S. and A. A. Kishk, "Invasive weed optimization and its features in electromagnetics," *IEEE Trans. Antennas Propag.*, Vol. 58, No. 4, 1269–1278, 2010.
38. Bhaskar, S. and A. K. Singh, "A compact meander line UHF RFID antenna for passive tag applications," *Progress In Electromagnetics Research M*, Vol. 99, 57–67, 2021.
39. Rahmat-Samii, Y., J. M. Kovitz, and H. Rajagopalan, "Nature-inspired optimization techniques in communication antenna designs," *Proceedings of the IEEE*, Vol. 100, No. 7, 2132–2144, Jul. 2012.